Journal of The Electrochemical Society, **157** (3) P23-P27 (2010)
0013-4651/2010/157(3)/P23/5/$28.00 © The Electrochemical Society

Rapid Fabrication of Cylindrical Colloidal Crystals and Their Inverse Opals

Chun-Han Lai, Yi-Jui Huang, Pu-Wei Wu,[*,z] and Li-Yin Chen

Department of Materials Science and Engineering, National Chiao Tung University, Hsin-Chu 300, Taiwan

We employed an electrophoretic deposition technique to prepare cylindrical colloidal crystals (CCCs) from polystyrene (PS) microspheres of 460 and 660 nm diameters using a carbon fiber (CF) with 7 μm diameter as the substrate. Measurements on the CCC diameter demonstrated growth rates that slowed down as time progressed. Scanning electron microscope images confirmed that the CCCs of 460 nm microspheres formed a face-centered cubic close-packed lattice, whereas an amorphous structure appeared for the CCCs of 660 nm. Subsequently, both CCCs underwent a potentiostatic electroplating to deposit Ni into the interstitial voids among the PS microspheres. After chemical removal of the PS microspheres, we fabricated cylindrical inverse opals (CIOs) in various diameters. As expected, better crystallinity was found on the CIOs of 460 nm microspheres as opposed to the 660 nm ones. The electrical resistivity for both CIOs exhibited a substantial reduction over that of the CF. Our CCCs and CIOs revealed considerable structure stability with excellent surface uniformity. The fabrication scheme enables rapid preparations of CCCs and CIOs in desirable lengths and diameters.
 [DOI: 10.1149/1.3280268]

Manuscript submitted October 5, 2009; revised manuscript received December 1, 2009. Published January 19, 2010.

There have been considerable interests to prepare colloidal crystals and their inverse opals for applications in photonic crystals, sensors, batteries, and displays.[1-5] Conventional methods to construct the colloidal crystals involve assembly of submicrometer microspheres, such as polystyrene (PS) and SiO_2 at various diameters in designated three-dimensional arrangements.[6,7] Many techniques are explored to direct the assembly of microspheres in desirable forms for colloidal crystals. For example, physical confinement, gravitational sedimentation, spin-coating, and electrophoretic deposition (EPD) have been widely studied.[8-11] Among them, the EPD is recognized for easy setup and facile assembly on a variety of conductive substrates.[12-14]

To fabricate the inverse opals, proper assembly of the colloidal crystals is a prerequisite. Subsequently, the interstitial voids among the microspheres are filled with targeted materials or precursors for chemical transformation. To date, a rich variety of filling methods, including melt infiltration, sol–gel chemistry, chemical vapor deposition, in situ polymerization, chemical bath deposition, infiltration of nanoparticles, and electrodeposition, have been reported.[15-28] Afterward, the colloidal template is often chemically or thermally removed to render a periodic macroporous structure with an interconnected skeleton. An extensive review on the morphological control for the inverse opals is provided recently by Stein et al.[29]

The earliest example of inverse opals via the electrodeposition route was CdS and CdSe for their relatively high refractive indexes for photonic crystal applications.[28,30] Later, electrodepositions for metallic inverse opals have been demonstrated to produce three-dimensionally ordered macroporous (3DOM) materials. For example, 3DOM, including Ni, Au, Co, Fe, and their alloys have been demonstrated.[31,32] In addition to metals, oxide inverse opals such as PbO_2, IrO_2, and ZnO have been demonstrated.[33-35] Because the EPD is conducted in a solution state, it is suitable to fabricate the inverse opals by a similar electroplating route. In addition, the growth rates for the EPD and electroplating are known for simple adjustments by varying the applied voltage and process time. Therefore, combining these two techniques, a rapid fabrication of colloidal crystals and their inverse opals becomes feasible.

The substrates used for the colloidal crystals and their inverse opals are often in planar forms, such as Si and indium tin oxide glass.[36,37] In contrast, cylindrical colloidal crystals (CCCs) and cylindrical inverse opals (CIOs) have received fewer studies.[38-41] For example, Lin et al. adopted a microfluid to deposit poly(methyl methacrylate) microspheres within a two-hole optical fiber to form in-fiber colloidal photonic crystals.[38] In addition, Míguez et al. assembled SiO_2 microspheres within the microchannels followed by Si deposition to produce Si inverse opals.[39] Unfortunately, in those researches, the sizes for the CCCs and CIOs were limited by the template they selected. In addition, their fabrication approaches entailed tedious and time-consuming steps to complete. In contrast, the EPD process and electroplating are versatile for tunable sizes and adjustable rates. For making the CCCs and CIOs, the thickness can be readily increased with deposition time, and their length is simply controlled by substrate selections.

The applications of EPD in a cylindrical configuration were demonstrated earlier for solid oxide fuel cells and supercapacitors.[42,43] However, the practice of EPD for CCCs has not been reported yet. Recently, we combined the EPD and electroplating techniques to fabricate planar colloidal crystals and inverse opals on a Si substrate.[44] After deliberate adjustments in the relevant processing parameters, we demonstrated the exact control in the deposit thickness. In this work, we adopt a similar approach to prepare the CCCs and CIOs in various diameters using a carbon fiber (CF) as the substrate.

Experimental

PS microspheres with 660 and 460 nm diameters were synthesized via an emulsifier-free emulsion polymerization process and were subsequently used to prepare the CCCs. For 660 nm microspheres, 33 mL of styrene monomer and 0.25 g $K_2S_2O_8$ were mixed in 325 mL deionized (DI) water. The polymerization took place at 70°C under N_2 for 18 h. For the 460 nm ones, 50 mL styrene and 0.25 g $NaHCO_3$ were mixed in 450 mL DI water for 1 h followed by the addition of 0.25 g $K_2S_2O_8$. The polymerization was conducted at 75°C under N_2 for 18 h. For 660 and 460 nm microspheres, their standard deviations were 16.4 and 10.1 nm, respectively.

In the fabrication of CCCs, an EPD technique was adopted, in which a CF with a diameter of 7 μm and a length of 2.5 cm was used as the substrate. The CF was carefully separated from a strand of CFs (Torayca-T300) after degreasing and proper cleaning. A Cu tape and Ag conductive gel were applied to establish electrical contact to the CF. To prepare an EPD suspension, 0.2 g microspheres (660 nm) were mixed in 100 mL 99.5 wt % ethanol followed by ultrasonication and stirring for 5 h. Alternatively, 0.25 g microspheres (460 nm) were used. These PS amounts were selected to obtain the necessary stability in suspensions that rendered a suitable EPD rate for the CCCs. The zeta potentials for the 460 and 660 microsphere suspensions were –65.19 and –61.17 mV, respectively. Because the microspheres carried negative charges, the CF served as the anode during electrophoresis. The conductivities for the 460 and 660 nm suspensions were 0.0332 and 0.0045 mS/cm.

Figure 1a illustrates the experimental setup for the EPD process. As shown, two electrodes were arranged vertically in a coaxial con-

* Electrochemical Society Active Member.
z E-mail: ppwu@mail.nctu.edu.tw

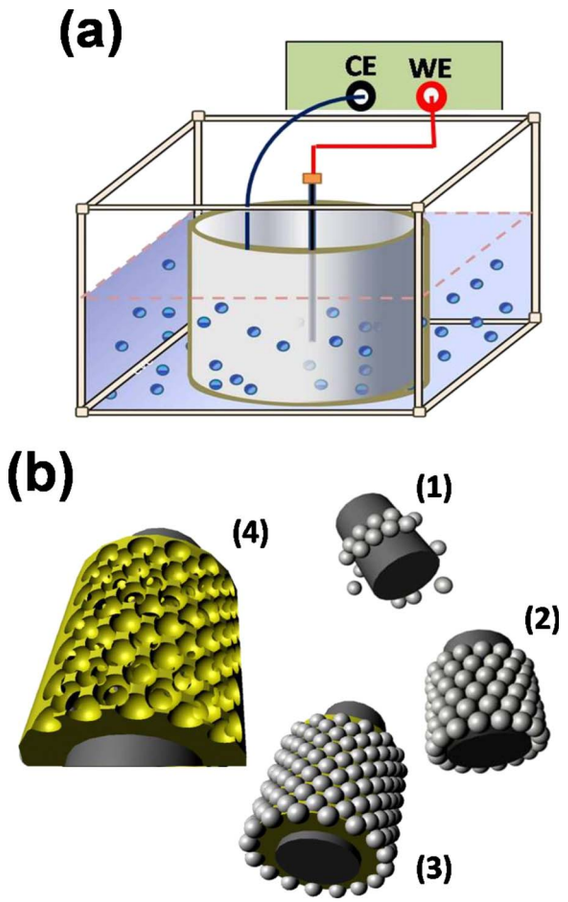

Figure 1. (Color online) Schematic diagrams for (a) experimental setup in EPD process and (b) processing steps involved for CCCs and CIOs in (1) EPD of PS microspheres, (2) electrophoretic assembly of PS colloidal crystals, (3) electrodeposition of Ni among the interstitial voids of the PS microspheres, and (4) chemical removal of PS microspheres to fabricate Ni inverse opals.

figuration. The CF, which served as the working electrode, was immersed in the suspension at 1 cm depth. A stainless steel (A304) tube with a length of 3 cm (1 cm under suspension) and a diameter of 4.6 cm was used as the counter electrode. A voltage of 10 V was imposed, resulting in an electric field of 4.35 V/cm in a radial direction. Afterward, the samples were removed and dried for 20 min. Both the EPD and drying of CCCs were performed at 25°C.

To fabricate the CIOs, the CCCs were immersed in a Ni plating solution including $NiSO_4 \cdot 6H_2O$ (130 g/L), $NiCl_2 \cdot 6H_2O$ (30 g/L), H_3BO_3 (18 g/L), and H_2O_2 (3 mL/L). The electrodeposition was carried out at 1 V and 25°C with a Ni plate (20 cm^2) used as the counter electrode. The distance between the Ni plate and CCCs was 2 cm. After Ni deposition, the CIOs were cleaned with DI water, and the embedded microspheres were carefully etched away by immersing the samples in an ethyl acetate (95 wt %) solution for 2 h. Figure 1b provides a schematic diagram for the fabrication steps involved.

Morphologies for the CCCs and CIOs were observed by a scanning electron microscope (SEM, JEOL-LSM-6700F). Optical images were obtained using a digital charge-coupled device camera (CY-100A) coupled with an optical microscope (Olympus CX41). A four-point probe (Keithley 2400) on the CIOs was performed to determine their electrical resistivity. During the measurements, the current was recorded under a bias swing from 0 to 1.5 V at 0.05 V intervals.

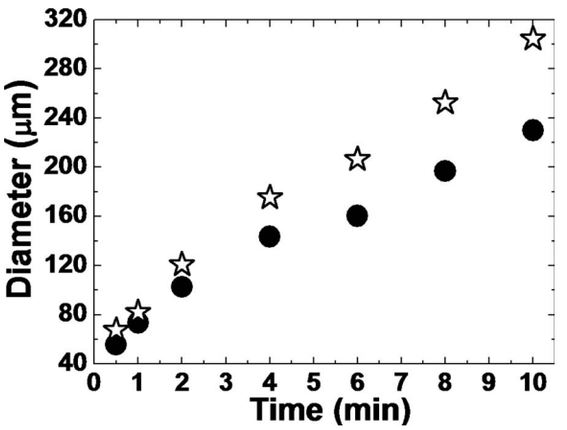

Figure 2. Growth of CCC diameter as a function of EPD time for microspheres of 460 (☆) and 660 nm (●). The concentrations for the 460 and 660 nm microspheres were 2.5 and 2.0 g/L, respectively. The applied voltage for the EPD was 10 V with a distance of 4.6 cm between the working and counter electrodes.

Results and Discussion

Figure 2 presents the relation for the CCC diameter as a function of EPD time in suspensions of 460 and 660 nm microspheres. For both samples, the diameter of CCCs increased with EPD time, and their increments slowed as time progressed. Reduction in the growth rate was expected because as the CCC diameter became larger, it took more microspheres to cover the entire perimeter. The known "screening effect" also rendered a diminishing driving force as the EPD continued. The respective EPD rates for the 460 and 660 nm CCCs were initially 0.322 and 0.301 μm/s, which suggested that each monolayer coverage required 2–3 s to complete. A faster deposition rate was observed for the 460 nm microspheres as opposed to the 660 nm ones. This is possibly attributed to a higher mass loading in the 460 nm suspension.

The surface morphologies for the CCCs of 460 and 660 nm microspheres are shown in Fig. 3. As shown in Fig. 3a, the sample underwent 30 s of EPD, resulting in a diameter of 67.3 μm. This corresponded to 76–77 layers of 460 nm microspheres atop the CF core. Obviously, the CCCs revealed considerable surface uniformity without undesirable valleys and islands. The microspheres formed a close-packed face-centered cubic lattice (111) with scattered vacancies. In addition, grain boundaries were observed because their presence was necessary to accommodate the cylindrical substrate. The CCCs of 660 nm microspheres, shown in Fig. 3b, demonstrated a random structure. This sample was prepared after 45 s of EPD that led to a diameter of 64.7 μm. This amounted to 50–51 layers of 660 nm microspheres. The reason we observed that improved crystallinity for the 460 nm CCCs over the 660 nm ones was the smaller microspheres can pack better around a curved substrate than the larger microspheres for a given fiber curvature.

To fabricate defectless CIOs, the proper assembly of microspheres on a cylindrical substrate is essential because it plays a crucial role in the subsequent electrodeposition process. Because we adopted a constant 1 V for the Ni plating, the resulting current was inversely proportional to the sum of the electrolyte internal resistance (iR) loss and Ni^{2+}/Ni charge-transfer resistance. As the Ni^{2+}/Ni reduction and growth were well known, its charge-transfer resistance was considered relatively unchanged in our process. Therefore, variation in the electrolyte iR greatly affected the plating current, which determined the deposit thickness and uniformity. Hence, CCCs in ordered or random structures were expected to engender a substantial difference in the electrolyte iR because their respective electrolyte percolation distance was not the same. In our earlier experience of fabricating planar inverse opals with controlled

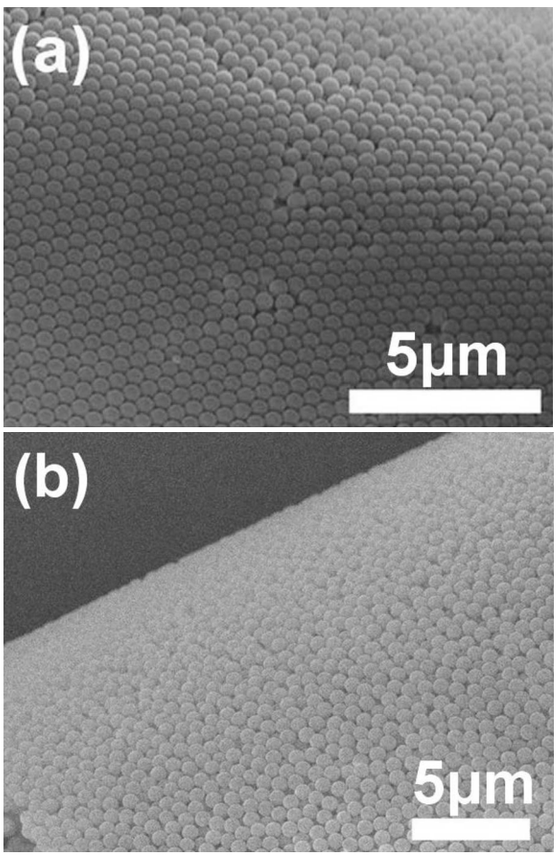

Figure 3. SEM images for CCCs of (a) 460 and (b) 660 nm PS microspheres.

thickness, we chose colloidal crystals in finite layers to minimize the electrolyte iR effect.[44] Following identical considerations, we selected the CCCs from Fig. 3 to carry out Ni electrodeposition for CIOs.

Figure 4 presents the plot of current density as a function of

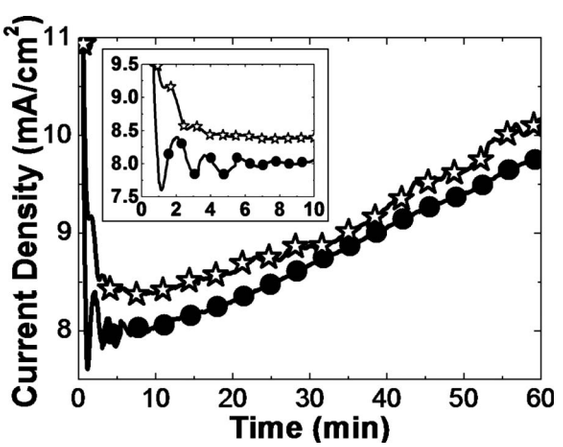

Figure 4. Variation in current density as a function of plating time for CCCs of 460 (☆) and 660 nm (●) microspheres. The inset picture presents the current fluctuation in the initial stage. The CCC diameters for electroplating for the 460 and 660 nm ones were 67.3 and 64.7 μm, respectively. The distance between the working and counter electrodes was 2 cm with an applied voltage of 1 V at 25°C.

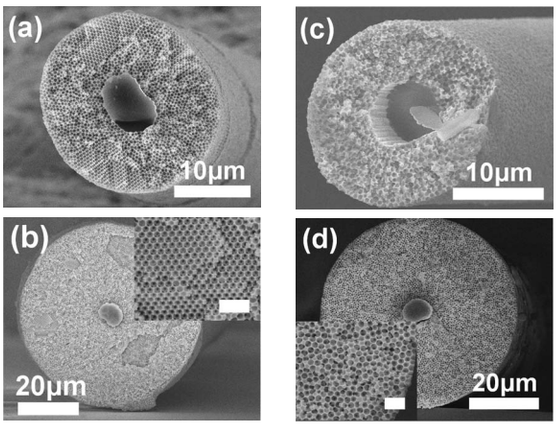

Figure 5. SEM images for CIOs of 460 nm microspheres after (a) 10 and (b) 60 min Ni plating as well as CIOs of 660 nm microspheres after (c) 10 and (d) 60 min Ni plating. The inset pictures are the high magnification images with scale bars of 2 μm. The distance between the working and counter electrodes was 2 cm with an applied voltage of 1 V at 25°C.

plating time using samples from Fig. 3. As shown, both currents initially revealed a sudden drop but moved to larger values afterward. Current oscillations appeared within the first 6 min. A similar behavior was previously observed by Hao et al. in their studies of magnetic properties associated with planar inverse opals.[45] They attributed this unique pattern to the variation in the deposition area as Ni filled the interstitial voids. After 6 min, these current fluctuations were subdued, and steady increments occurred, indicating a uniform and consistent movement in the Ni front. Because the CCCs of 460 nm demonstrated better crystallinity over that of 660 nm, its electrolyte percolation distance was shorter, leading to a slightly larger current over the entire plating process.

Figure 5 presents the SEM images for the CIOs at various plating times. Figure 5a and b shows the CIOs of 460 nm microspheres after 10 and 60 min of Ni plating. Their respective thicknesses for the inverse structure (excluding CF) were 8.14 and 27.09 μm. Because the CF itself was not perfectly cylindrical, the CCCs and corresponding CIOs demonstrated a moderate disordering near the CF. However, a significantly improved packing with ordered pore arrays was observed far from the CF. It is because the circumference was sufficiently large to assume a near planar case for the incoming microspheres to assemble in a close-packed arrangement. This behavior was confirmed by the inset image of Fig. 5b, which shows hexagonal arrays in perfect order. This disorder–order transition occurred earlier at 460 nm suspension than the 660 nm one. Figure 5c and d shows the CIOs of 660 nm microspheres after 10 and 60 min Ni plating. Their corresponding thicknesses for the inverse structure (excluding CF) were 6.88 and 23.88 μm, respectively. Apparently, both samples exhibited disordered packing arrays. A high magnification image in the inset of Fig. 5d confirmed its random nature. This poor crystallinity was traced back to the CCCs that already displayed a defective packing. In our experiments, the CCCs of 660 nm microspheres required a thickness of 68.3 μm to reach a close-packed structure. Unfortunately, this thickness was too large to allow a suitable electrolyte percolation for a desirable CIO formation.

As electroplating is known for its simple control to obtain a desirable deposit thickness, the diameter for the CIOs could be manipulated by adjusting the plating time. Figure 6 presents the evolution of CIO diameter at various plating times. Their growth rates were 0.38 and 0.32 μm/min for the CIOs of 460 and 660 nm, respectively. The reason for the CIOs of 460 nm microspheres to exhibit a faster growth rate was its close-packed structure, which allowed 26% voids among microspheres. In contrast, the CIOs of 660 nm contained a larger percentage of voids that required more Ni to fill in.

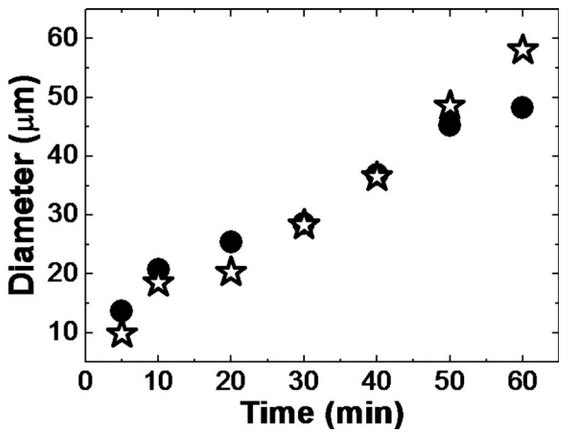

Figure 6. Growth of CIO diameter as a function of Ni plating time for microspheres of 460 (☆) and 660 nm (●).

Because we obtained the CIOs in different diameters, it would be interesting to determine their respective electrical resistivity. As both the CF and Ni are conductors, linear current–voltage profiles confirmed ohmic contacts between the CIOs and probes. Their slopes were used to derive the resistivity assuming that the CIOs were homogeneous materials made of CF and porous Ni. Figure 7 provides the resistivity values of CIOs in different diameters as well as the CF itself. As shown, the CF exhibited a resistivity of 4.647×10^{-5} Ω m. The CIOs demonstrated an increasing resistivity with a larger diameter. However, all their values were below 1.331×10^{-5} Ω m. In addition, at an identical diameter, there was a negligible difference between the CIOs of 460 and 660 nm microspheres.

Figure 8 provides the optical images for the CIOs of 460 and 660 nm microspheres with insets showing their respective CCCs. Both CCCs appeared opaque, and the black CF was invisible. After the Ni plating and PS removal, the CIOs became considerably darkened. Apparently, the CCCs and CIOs demonstrated impressive mechanical strength and surface uniformity as their structure was nicely maintained over the entire length (1 cm). In the SEM observations, the 460 nm CCCs revealed a polycrystalline structure with individual grains approximately 10–15 μm in size. But the 660 nm CCCs demonstrated an amorphous structure instead. However, both samples did not exhibit notable cracks for the sample length of 1 cm.

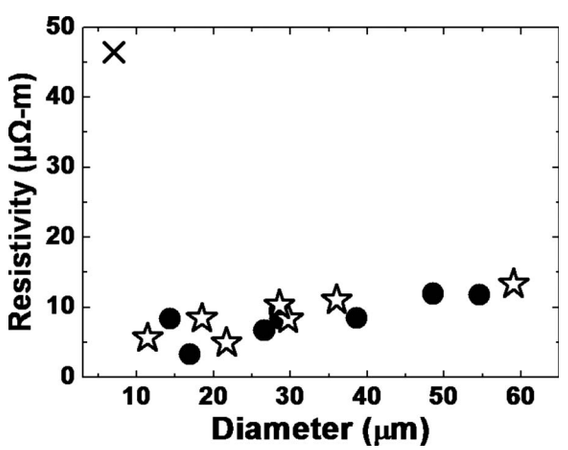

Figure 7. Resistivity values for CF (×) as well as CIOs of 460 (□) and 660 nm (●) microspheres.

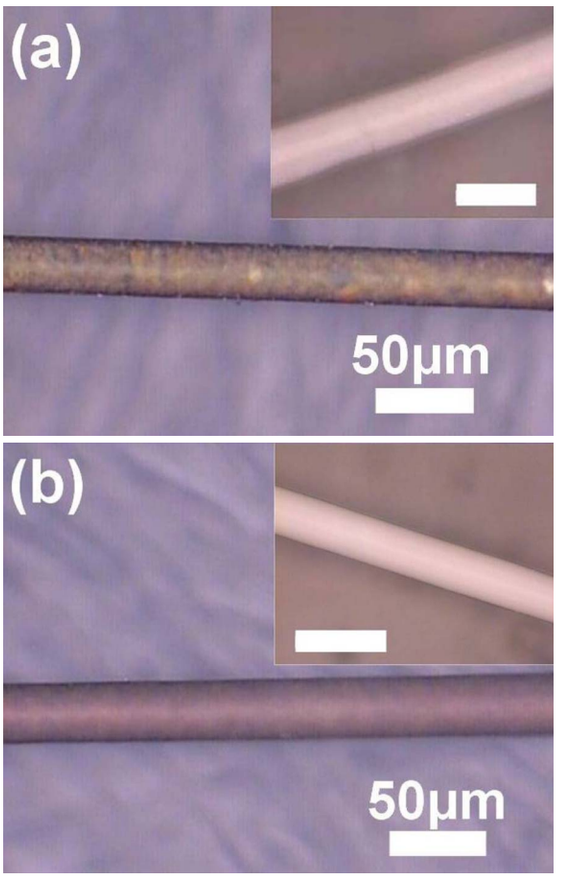

Figure 8. (Color online) Optical images for CIOs of (a) 460 and (b) 660 nm microspheres. Insets are their corresponding CCC images with scale bars of 100 μm.

Our fabrication scheme allows facile preparations of CCCs and CIOs in superb structural integrity. In addition, both their diameters and lengths could be deliberately designed to suit purposed applications. Moreover, it is possible to replace the CF with other conductive substrates at different diameters. This diversity in the sample fabrication might lead to unique CCC and CIO structures for applications in the future.

Conclusions

The EPD process was used to construct the CCCs from PS microspheres of 460 and 660 nm using the CF as the substrate. Measurements on the CCC diameter determined growth rates that slowed down as EPD progressed. SEM images on the CCC surface morphologies indicated that the 460 nm microspheres were able to form a close-packed structure, whereas a defective one occurred for the 660 nm microspheres. Electroplating at 1 V was conducted to deposit the Ni among the interstitial voids in CCCs. We obtained the CIOs in various diameters by adjusting the relevant Ni plating time. Improved crystallinity for the CIOs of 460 nm microspheres was observed as opposed to the 660 nm ones. For both samples, the electrical resistivity showed a marked reduction over that of the CF. Both the CCCs and CIOs revealed a considerable structure stability with a superb surface uniformity.

Acknowledgment

The authors are grateful to Professor Chih Chen and Professor George Tu for assisting in laboratory equipment.

National Chiao Tung University assisted in meeting the publication costs of this article.

References

1. Y. Xia, B. Gates, and Z. Y. Li, *Adv. Mater.*, **13**, 409 (2001).
2. Y. S. Lin, Y. Hung, H. Y. Lin, Y. H. Tseng, Y. F. Chen, and C. Y. Mou, *Adv. Mater.*, **19**, 577 (2007).
3. I. D. Kim, A. Rothschild, D. J. Yang, and H. L. Tuller, *Sens. Actuators B*, **130**, 9 (2008).
4. H. W. Yan, S. Sokolov, J. C. Lytle, A. Stein, F. Zhang, and W. H. Smyrl, *J. Electrochem. Soc.*, **150**, A1102 (2003).
5. W. N. Ng, C. H. Leung, P. T. Lai, and H. W. Choi, *Nanotechnology*, **19**, 255302 (2008).
6. Q. F. Yan, L. K. Teh, Q. Shao, C. C. Wong, and Y. M. Chiang, *Langmuir*, **24**, 1796 (2008).
7. D. Yamamoto, H. Munakata, and K. Kanamura, *J. Electrochem. Soc.*, **155**, B303 (2008).
8. Á. Blanco, E. Chomski, S. Grabtchak, M. Ibisate, S. John, S. W. Leonard, C. Lopez, F. Meseguer, H. Míguez, J. P. Mondia, et al., *Nature (London)*, **405**, 437 (2000).
9. Á. Blanco and C. López, *J. Mater. Chem.*, **16**, 2969 (2006).
10. G. I. N. Waterhouse and M. R. Waterland, *Polyhedron*, **26**, 356 (2007).
11. C. H. Chan, C. C. Chen, C. K. Huang, W. H. Weng, H. S. Wei, H. Chen, H. T. Lin, H. S. Chang, W. Y. Chen, W. H. Chang, et al., *Nanotechnology*, **16**, 1440 (2005).
12. R. Szamocki, S. Reculusa, S. Ravaine, P. N. Bartlett, A. Kuhn, and R. Hempelmann, *Angew. Chem., Int. Ed.*, **45**, 1317 (2006).
13. K. S. Napolskii, A. Sinitskii, S. V. Grigoriev, N. A. Grigorieva, H. Eckerlebe, A. A. Eliseev, A. V. Lukashin, and Y. D. Tretyakov, *Physica B*, **397**, 23 (2007).
14. Y. W. Chung, I. C. Leu, J. H. Lee, and M. H. Hon, *J. Electrochem. Soc.*, **156**, E91 (2009).
15. L. Xu, W. Zhou, M. E. Kozlov, I. I. Khayrullin, I. Udod, A. A. Zakhidov, R. H. Baughman, and J. B. Wiley, *J. Am. Chem. Soc.*, **123**, 763 (2001).
16. S. L. Kuai, G. Bader, and P. V. Ashrit, *Appl. Phys. Lett.*, **86**, 221110 (2005).
17. J. Y. Shiu, C. W. Kuo, and P. L. Chen, *J. Am. Chem. Soc.*, **126**, 8096 (2004).
18. L. A. Woldering, A. M. Otter, B. H. Husken, and L. V. Willem, *Nanotechnology*, **17**, 5717 (2006).
19. W. L. Min, P. Jiang, and B. Jiang, *Nanotechnology*, **19**, 475604 (2008).
20. Y. J. Huang, C. H. Lai, and P. W. Wu, *Electrochem. Solid-State Lett.*, **11**, P20 (2008).
21. N. V. Dziomkina, M. A. Hempenius, and G. J. Vancso, *Adv. Mater.*, **17**, 237 (2005).
22. R. C. Hayward, D. A. Saville, and I. A. Aksay, *Nature (London)*, **404**, 56 (2000).
23. L. Besra and M. L. Liu, *Prog. Mater. Sci.*, **52**, 1 (2007).
24. M. W. Perpall, K. P. U. Perera, J. DiMaio, J. Ballato, S. H. Foulger, and D. W. Smith, *Langmuir*, **19**, 7153 (2003).
25. X. Yang, Y. Jin, Y. Zhu, L. Tang, and C. Li, *J. Electrochem. Soc.*, **155**, J23 (2008).
26. H. Yan, C. F. Blanford, B. T. Holland, M. Parent, W. H. Smyrl, and A. Stein, *Adv. Mater.*, **11**, 1003 (1999).
27. O. D. Velev, P. M. Tessier, A. M. Lenhoff, and E. W. Kaler, *Nature (London)*, **401**, 548 (1999).
28. P. V. Braun and P. Wiltzius, *Nature (London)*, **402**, 603 (1999).
29. A. Stein, F. Li, and N. R. Denny, *Chem. Mater.*, **20**, 649 (2008).
30. P. V. Braun and P. Wiltzius, *Adv. Mater.*, **13**, 482 (2001).
31. L. Xu, W. L. Zhou, C. Frommen, R. H. Baughman, A. A. Zakhidov, L. Malkinski, J. Q. Wang, and J. B. Wiley, *Chem. Commun. (Cambridge)*, **2000**, 997.
32. P. N. Bartlett, M. A. Ghanem, I. S. El Hallag, P. de Groot, and A. Zhukov, *J. Mater. Chem.*, **13**, 2596 (2003).
33. P. N. Bartlett, T. Dunford, and M. A. Ghanem, *J. Mater. Chem.*, **12**, 3130 (2002).
34. J. Hu, M. Abdelsalam, P. Bartlett, R. Cole, Y. Sugawara, J. Baumberg, S. Mahajan, and G. Denuault, *J. Mater. Chem.*, **19**, 3855 (2009).
35. H. Yan, Y. Yang, Z. Fu, B. Yang, L. Xia, S. Fu, and F. Li, *Electrochem. Commun.*, **7**, 1117 (2005).
36. T. H. Chen, T. Y. Tsai, K. C. Hsieh, S. C. Chang, N. H. Tai, and H. L. Chen, *Nanotechnology*, **19**, 465303 (2008).
37. Y. W. Chung, I. C. Leu, J. H. Lee, J. H. Yen, and M. H. Hon, *J. Electrochem. Soc.*, **154**, E77 (2007).
38. Y. K. Lin, P. R. Herman, and W. Xu, *J. Appl. Phys.*, **102**, 073106 (2007).
39. H. Míguez, S. M. Yang, N. Tétreault, and G. A. Ozin, *Adv. Mater.*, **14**, 1805 (2002).
40. J. H. Moon, S. Kim, G. R. Yi, Y. H. Lee, and S. M. Yang, *Langmuir*, **20**, 2033 (2004).
41. J. H. Moon, G. R. Yi, and S. M. Yang, *J. Colloid Interface Sci.*, **287**, 173 (2005).
42. H. Negishi, N. Sakai, K. Yamaji, T. Horita, and H. Yokokawa, *J. Electrochem. Soc.*, **147**, 1682 (2000).
43. J. Li and I. Zhitomirsky, *Mater. Chem. Phys.*, **112**, 525 (2008).
44. Y. J. Huang, C. H. Lai, P. W. Wu, and L. Y. Chen, *Mater. Lett.*, **63**, 2393 (2009).
45. Y. W. Hao, F. Q. Zhu, C. L. Chien, and P. C. Searson, *J. Electrochem. Soc.*, **154**, D65 (2007).